Theory and performance of an adaptive current tomography system

Clin. Phys. Physiol. Meas., 1988, Vol. 9, Suppl. A, 35–41. Printed in Great Britain

Theory and performance of an adaptive current tomography system

D G Gisser†, D Isaacson‡ and J C Newell§

†Electrical, Computer and Systems Engineering Department, RPI Troy, New York 12180, USA

‡Mathematics Department, RPI Troy, New York 12180, USA and Visiting Research Fellow, General Electric Corporation, Research and Development, Schenectady, New York 12301, USA

§Biomedical Engineering Department, RPI Troy, New York 12180, USA

Abstract. It has been shown that there exists an optimum set of current patterns for distinguishing one conductivity distribution from another. Since the optimum set of current patterns depends on the conductivity distribution being imaged it must be determined for each object being imaged. This paper describes how these current patterns may be determined and describes a system for achieving this in practice.

1. Introduction

We have recently presented a theoretical description of an adaptive process for finding the best current patterns to distinguish one conductivity distribution, $\sigma(p)$, from another, $\tau(p)$ (Isaacson 1986, Gisser *et al* 1987a, b). The theory was given and the process analytically proven to converge for arbitrary geometries and dimensions in Gisser *et al* 1987b.

Here we given a brief description of this process. We then describe an adaptive current tomography system (ACT 1) we have built that can carry out this process for two- and three-dimensional bodies.

We conclude with a description of some experiments that have validated the theory for two-dimensional test phantoms.

2. Theory and description of adaptive process

Let L electrodes, $e_l, l = 1, \ldots, L$ of area $f\Delta$ be placed on a surface S. Here

$$\Delta = \text{Area}(S)/L$$

and f is the fraction of S covered by the electrodes. Assume the surface S surrounds a body B whose internal conductivity at a point p is $\sigma(p)$.

For $l = 1,2, \ldots, L$; I_l^k denotes the kth current applied to the lth electrode and V_l^k denotes the kth voltage that results on the lth electrode.

The phantom used in these experiments is a cylinder of radius r_0 with L electrodes placed on its sides of height h and width

$$w = f \cdot r_0 \cdot 2\pi/L$$

When the cylinder is filled with saline of conductivity σ_0 to a height h and currents I_l^k are applied to the electrode e_l centred at $\theta_l = l.2\pi/L$ a current density $j^k = j^k(\theta)$, that is independent of depth, results on S.

0951-7979/88/0A0035 + 07$02.50

Generally this current density has a Fourier series representation

$$j^k(\theta) = \sum_{n=1}^{\infty} C_n^k \cos n\theta + S_n^k \sin n\theta$$

where

$$C_n^k = \frac{1}{\pi} \int_0^{2\pi} j^k(\theta) \cos n\theta \, d\theta$$

and

$$S_n^k = \frac{1}{\pi} \int_0^{2\pi} j^k(\theta) \sin n\theta \, d\theta$$

This current density results in voltages $V_l^k(\sigma_0)$.

Let $V_l^k(\tau)$ denote the voltages that the kth current would produce on the lth electrode when a cylinder of radius r, depth h, and conductivity σ is centred in the previous saline filled phantom.

The voltage difference between homogeneous and centred phantoms, δV_l^k, is then approximately given by

$$\delta V_l^k = V_l^k(\sigma_0) - V_l^k(\tau)$$

$$\delta V_l^k \approx \sum_{n=1}^{\infty} p_l (C_n^k \cos n\theta_l + S_n^k \sin n\theta_l) \tag{1}$$

where

$$p_n = (r_0/\sigma_0 n) \cdot (2\mu R^{2n}) / (1 + \mu R^{2n})$$

and

$$\mu \equiv (\sigma - \sigma_0) / \sigma \times \sigma_0)$$
$$R \equiv r/r_0$$

This formula (1) was compared with experiments for the currents (in mA):

$$I_l^1 = 5 \cos k\theta_l$$

$$I_l^2 = \begin{bmatrix} 5 \text{ if } l = 1 \\ -5 \text{ if } l = 2 \\ 0 \text{ if } l = 1 \text{ or } 2 \end{bmatrix}$$

$$I_l^3 = \begin{bmatrix} 5 \text{ if } l = 1 \\ -5 \text{ if } l = 17 \\ 0 \text{ if } l = 1 \text{ or } 17 \end{bmatrix}$$

The cosine pattern I^1 yields the largest voltage differences and enables us to distinguish smaller centred targets than the other patterns.

A centred cylindrical conductor of radius r can be distinguished from a uniform background by the current pattern I^k only if the maximum voltage difference, $\max_l |\delta V_l^k| \geq \epsilon_v$, where ϵ_v is the smallest voltage difference the system can reliably measure.

When L is large and f is approximately one, it follows from equation (1) that for the cosine current pattern I^1 this is the case if

$$r \geq r_b \equiv \frac{(f\pi h \sigma_0 \epsilon_v / 5L)^{1/2} r_0}{5L} \tag{2}$$

For the single current I^2 applied between a pair of adjacent electrodes:

$$r \geq r_a = [4 \sin(f\pi/L)\sin(\pi/L)/\pi]^{-1/2} r_b \tag{3}$$

For the single current I^3 applied between opposite electrodes:

$$r \geq r_p = [4 \sin(f\pi/L)/\pi]^{-1/2} r_b \tag{4}$$

Here $2r_b$, $2r_a$ and $2r_p$ yield the diameters of the smallest centred, conducting cylinders that can be distinguished from a uniform background. When $r_0 = 15$ cm, $\sigma_0^{-1} = 350\ \Omega$ cm, $L = 32$, h = 3.6 cm and $\epsilon_v = 5$ mV the respective diameters are 0.9, 8.3 and 2.6 cm.

In general, we measure the ability of a current pattern $I^k = (I_1^k,\ldots,I_L^k)$, to distinguish between two conductivities σ and τ by a single number, the 'distinguishability δ' where

$$\delta = \delta(\sigma,\tau;I^k)$$

$$\delta \equiv \frac{\left[\sum_{l=1}^{L} (V_l^k(\sigma) - V_l^k(\tau))^2\right]^{1/2}}{\left[\sum_{l=1}^{L} (I_l^k)^2\right]^{1/2}}$$

We define $I^\star$ to be a 'best' pattern of current to distinguish σ from τ if $I^\star$ maximises the distinguishability, *i.e.*

$$\delta(\sigma,\tau;I^\star) = \max_I \delta(\sigma,\tau;I)$$

For the previous example, it can be proven that I^1 is a 'best' pattern. In general the best pattern depends on σ and τ and cannot be known in advance.

An adaptive process for producing the 'best' I to distinguish σ from τ is:

(1) Guess any I^k for $k = 0$.

(2) Measure or compute $V^k(\sigma)$ and $V^k(\tau)$.

(3) Compute

$$\delta V^k \equiv V^k(\sigma) - V^k(\tau)$$

$$\|\delta V^k\| \equiv \left[\sum_{l=1}^{L} (\delta V_l^k)^2\right]^{1/2}$$

and

$$I^{k+1} = \delta V^k / \|\delta V^k\|$$

(4) If $\|I^{k+1} - I^k\| \leq$ (minimum current difference specifiable) stop, otherwise set $k = k + 1$, and go to 2.

In order to be able to produce these 'best' current patterns, we designed and built the instrument, ACT 1, described in the next section.

3. Adaptive current tomograph — ACT 1

Here we describe the two-dimensional test prototype adaptive current tomography system. This test system consists of a 32-electrode array around a mock thorax which was used to obtain the data reported herein.

The prototype tomograph contains 32 independent current generators all controlled by a microcomputer. Each current generator produces a 12 kHz current having an amplitude of zero to 5.0 mA RMS with either polarity. Each current generator is separately addressable and can have its amplitude specified to within 0.05% (12-bit) accuracy by the computer. Since a 32-electrode array requires only 31 current generators, the 32nd generator is connected to a precision resistor and used as a calibration standard.

With any arbitrary current field imposed in the mock thorax by the current generators, the data of interest are the 32 voltages present on the electrodes. The system incorporates a 32-element multiplexer or switch, and a precision, polarity-sensitive voltmeter. This allows all voltages to be scanned rapidly under software control, and their magnitude stored by the computer. A second voltmeter is available to measure the quadrature voltage for reactance calculations.

An IBM PC AT is connected to the hardware system by a plug-in interface card (Data Translation DT2801). This card has two sets of 8-bit digital terminals all under software control and usable as both input and output terminals. It also contains 16 AD converter channels.

A program written in ASYST controls the hardware. First, on command of the computer program, a sequential set of 32 digital values and addresses is sent to the digital interface. These control the values and polarity of the AC currents delivered by the 32 current sources, which are sinusoidal, at 12 kHz. The time required to address all the current sources is called the 'set-up time'. The phantom under test has 32 electrodes, one of which is permanently designated the one tied to the common signal terminal. The other 31 are fed from the current sources. A phase-sensitive AC voltmeter is then connected to each of the 31 electrodes and the test resistor, in turn, and the values digitised and sent to the computer for storage, again through the interface card. The time required to measure all the electrode voltages for a particular current vector is called the 'scan time'. This is less than 1 s in the present instrument. At the end of the scan, the computer can deliver a second set of current values for the electrodes, and a second scan ensues. This procedure is repeated as many times as is required, and the total time is called the 'frame time'.

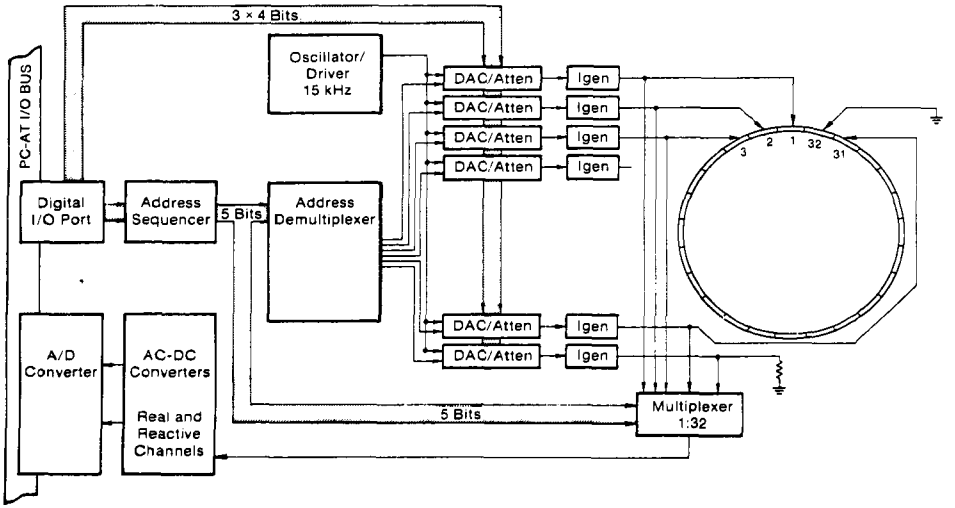

Figure 1. A block diagram of the adaptive current tomograph: ACT-1.

As seen in the block diagram, figure 1, the 32 values latched during the set-up time control the magnitude and polarity of the signals from the oscillator. The oscillator is amplitude-stabilised with a separate feedback, rectifier, and reference voltage system. Each of four buffers provides power to drive eight digital-to-analog converters, which operate as dual-polarity attenuators to provide a voltage to the voltage-to-current converters or current generators.

The 31 current sources are not of the simplest kind, with a floating load, because there must be a single common terminal for all. Instead, we use a circuit with three op-amps, rather than a single op-amp, thereby achieving a performance independent of the common mode rejection ratio of the devices. We also use capacitors to produce an AC-only current source with very low loop gain at DC.

The required presence of cables to the phantom under test places some capacitance in shunt with the electrodes on the phantom, thus shunting some of the current. We therefore couple to the phantom with multiconductor stripline, using every third conductor as the active connection and the adjacent two conductors are driven as a 'guard' to shield the central active lead.

The measuring system consists of a classical arrangement of a high-pass filter followed by a precision full-wave, phase-sensitive detector and then a low-pass filter. The ADC then takes a single sample of an essentially DC voltage.

4. Phantom

This system is designed for application to biological systems, the most promising of which is the thorax. For this reason, we have constructed an *in vitro* idealised model of the thorax. Thirty-two electrodes were fashioned from a titanium plate having a platinum-iridium surface. These electrodes were attached to the interior surface of a circular plastic container 30.0 cm (12 in) in diameter, 6.5 cm (2.4 in) deep. The electrodes are 28.4 mm wide, so that a 1.0 mm gap remains between electrodes, and extend throughout the depth of the container.

This circular container is then filled to a depth of 36 mm with saline solutions having different electrical conductivities over the range of interest. Targets with different geometries and conductivities are then placed in the bath. Metal or plastic targets are used for conductivities of infinity and zero. When conductivities similar to that of the bath are desired, mixtures of agar in saline are used to produce gelatin-like structures of desired geometry and conductivity, as described in Yorkey, *et al.* (1985).

5. Distinguishability experiments

Test phantoms composed of concentric cylindrical targets were placed in the cylindrical tank containing 385 Ω cm saline.

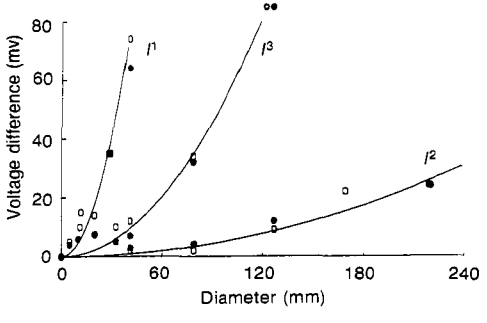

Figure 2. The distinguishability of inhomogeneities of various sizes for the three current patterns given in the text.

Figure 2 demonstrates the measured ability of the present system to distinguish inhomogeneities. The absolute value of the maximum difference between the voltages recorded with a target present and with no target present in the tank is plotted as a function of the diameter of the target. The target is placed in the centre of the tank. Three different patterns of current were tested. In the right-most, lower set of points, the current, I^2, is applied between two adjacent electrodes. The points shown were obtained using insulating (open circles) and conducting (closed circles) targets. The system can distinguish insulators or conductors from the homogeneous field with equal ability; the voltage differences are positive for insulators, negative for conductors. They are plotted here as absolute values for convenience. Voltage differences above 12 mV were seen when the target diameter was above 120 mm. The middle set of points was obtained using conducting and insulating

targets and a single current I^3, applied between a pair of diametrically opposed electrodes. Because this current pattern results in a larger current density through the centre of the tank where the target is located, a much larger voltage difference is seen. For example, a voltage difference of 96 mV is seen with a 120 mm diameter target. The voltage difference produced by these current patterns is to be compared with the significantly larger voltage differences produced by the best current pattern; I^1, shown in the left-most or upper points in figure 2. The ability of the present system to distinguish targets can be compared with the results obtainable by a pair of electrodes directly from figure 2. For example, using targets of 40 mm diameter, an electrode pair produces a voltage difference of only about 8-12 mV when diametrically opposed, and only 3 mV when adjacent. In contrast, a voltage difference of about 75 mV is obtained from the pair of electrodes at the maximum of the cosine waveform when a cosine pattern of currents is applied. Expressed alternatively, since the resolution of the present system's voltmeter is of the order of ± 2.5 mV (full scale is ± 5 V RMS) the upper-most points in figure 2 show that targets as small as 8-9 mm in diameter are detectable. It is important to note that these comparisons are all made for targets located at the centre of the tank, where their detection is most difficult. All of these current patterns will yield greater voltage differences as targets are placed closer to the appropriate electrodes. Since the present system adaptively produces the best current pattern, it will always have a distinguishability greater than that obtainable by either configuration of electrode pairs or by the cosine pattern, which is the best pattern only for concentric targets. The curves in Figure 2 give the results expected from the theoretical analysis of the experiment performed, obtained by evaluating the first Fourier coefficients of the current patterns I^k, and plotting the 1st term of $|\delta V_1^k|$ given by equation (1) for $k = 1,2,3$.

The smallest centred insulators distinguishable from a uniform background of 350 Ω cm saline for currents I^1, I^2, I^3 were found by placing successively smaller targets in the centre of the bath until the measured maximum voltage difference was approximately 5 mV.

The experimentally observed diameters 0.9, 8.2, and 2.6 cm agree closely with the values predicted by formulas (2)-(4).

Although the saline used in these experiments had a resistivity of 385 Ω cm, the value of resistivity used in formulas (1)-(4) was 350 Ω cm. The use of this 'effective' resistivity value permits us to model these experiments accurately with the simple formulas (1)-(4).

We have made a rudimentary test of ACT-1's ability to carry out the adaptive process given in section 2. Beginning with a deliberately poor choice of initial current pattern, I^2, and a central circular target, we allowed the second and subsequent current patterns used to be determined by the observed voltage pattern, obtained by subtracting the homogeneous voltage pattern from that observed with a target in the tank. The target used was a 41 mm diameter circular conductive target. The successive voltage patterns quickly approached a cosine, which is known to be the best current pattern for this simple case. The result extends the analytical results given in figures 1-6 of Gisser *et al* (1987a), which was based on theoretical calculations of the current pattern rather than on measurement of the physical phantom.

In a second test of the adaptive feature, we moved the target from the centre of the bath to a location at $\theta = 45°$, $R = 0.5$. Beginning with a poor choice of initial current pattern, that of two adjacent active electrodes at $\theta = 11°$ and $23°$, we again allowed the iterative scheme to determine subsequent current patterns. These successive current patterns are shown in figure 3. The voltage patterns, and the resulting current pattern for the next iteration approach a maximum on the electrode located nearest the target. The current pattern becomes smoother than the original guess, and is of relatively low amplitude where

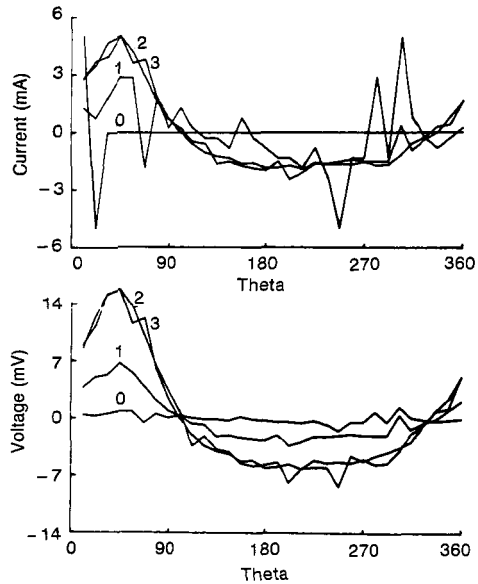

Figure 3. Successive current (top) and voltage (bottom) patterns computed for an object 41 mm in diameter positioned at $\theta = 45°$, $R = 0.5$.

the bath is homogeneous. In other words, the applied current is maximised near the inhomogeneity or target.

Acknowledgements

This paper was written while D Isaacson was a Visiting Research Fellow at GE Research and Development Centre. He would like to thank GE for the support and stimulating environment they provided.

We would also like to thank J Goble, T Gallagher, S Simske, K-S Cheng and L F Fuks for the considerable assistance they have provided in the performance of this research.

References

Gisser D G, Isaacson D and Newell J C 1987a Current topics in impedance imaging *Clin. Phys. Physiol. Meas.* **8** Suppl.A 39-46

_____ 1987b *Electric curent computed tomography and eigen-values I* RPI Report

Isaacson D 1986 Distinguishability of conductivities by electric computed tomography *IEEE Trans. Med. Imaging* **MI-5** 91-5

Yorkey Y T J, Webster J G and Tompkins W J 1985 Errors caused by contact impedance in impedance imaging *Proc. IEEE* 7th Conf. Eng. Med. Biol. pp 632-7